Combinatorial MAPLE gradient thin film assemblies signalling to human osteoblasts

2014 Biofabrication 6 035010

(http://iopscience.iop.org/1758-5090/6/3/035010)

IOP Publishing Biofabrication
Biofabrication 6 (2014) 035010 (9pp) doi:10.1088/1758-5082/6/3/035010

Combinatorial MAPLE gradient thin film assemblies signalling to human osteoblasts

Emanuel Axente[1,6], Felix Sima[1,6], Livia Elena Sima[1,2], Merve Erginer[3], Mehmet S Eroglu[4,5], Natalia Serban[1], Carmen Ristoscu[1], Stefana M Petrescu[2], Ebru Toksoy Oner[3] and Ion N Mihailescu[1]

[1] Lasers Department, National Institute for Lasers, Plasma and Radiation Physics, 409 Atomistilor Street, Magurele, Ilfov RO-77125, Romania
[2] Department of Molecular Cell Biology, Institute of Biochemistry, Romanian Academy, 296 Splaiul Independentei, 060031, Bucharest 17, Romania
[3] Department of Bioengineering, Marmara University, Goztepe, 34722 Istanbul, Turkey
[4] Department of Chemical Engineering, Marmara University, Goztepe, 34722 Istanbul, Turkey
[5] TUBITAK-UME, Chemistry Group Laboratories, 41471 Gebze, Kocaeli, Turkey

E-mail: lsima@biochim.ro

Received 27 November 2013, revised 10 March 2014
Accepted for publication 23 April 2014
Published 28 May 2014

Abstract

There is increased interest in smart bioactive materials to control tissue regeneration for the engineering of cell instructive scaffolds. We introduced combinatorial matrix-assisted pulsed laser evaporation (C-MAPLE) as a new method for the fabrication of organic thin films with a compositional gradient. Synchronized C-MAPLE of levan and oxidized levan was employed to assemble a two-compound biopolymer film structure. The gradient of the film composition was validated by fluorescence microscopy. In this study, we investigated the cell response induced by the compositional gradient using imaging of early osteoblast attachment and analysis of signalling phosphoprotein expression. Cells attached along the gradient in direct proportion to oxidized levan concentration. During this process distinct areas of the binary gradient have been shown to modulate the osteoblasts' extracellular signal-regulated kinase signalling with different propensity. The proposed fabrication method results in the preparation of a new bioactive material, which could control the cell signalling response. This approach can be extended to screen new bioactive interfaces for tissue regeneration.

Keywords: combinatorial MAPLE, polymer coatings, gradient levan-oxidized levan thin films, osteoblasts, ERK1/2 signalling

(Some figures may appear in colour only in the online journal)

1. Introduction

Fifty years after the fabrication of the first generation of inert implantable devices and thirty years after the first clinical use of second-generation bioactive orthopaedic and dental materials, a third-generation of biomaterials is required to trigger specific molecular responses of cells for tissue regeneration purposes [1]. Translation of *smart materials* into clinics [2] could further improve the quality-of-life for a continually aging population. Engineering the cell/biomaterial surface interface to control cell behaviour has important implications for the fabrication of *instructive environments* for tissue repair or as cell supports [3].

Bone tissue engineering has made use of a large variety of scaffolds designed to support osteoblast growth as well as function. While the vast majority of materials used to regenerate bone have been based on calcium phosphates, there have also been attempts to design extracellular matrix (ECM)-inspired materials to mimic the natural environment of the bone (reviewed in [4]). These materials provide extracellular microenvironments for controlled differentiation of osteoprogenitor cells [5].

[6] Authors with equal contribution.

There are several strategies to develop materials that control stem cell differentiation [6] to meet the requirements for use in clinical applications [7]. It would be tremendous progress to obtain synthetic *niches* designed to recapitulate the spatial and temporal control of gene expression known to regulate cell fate *in vivo* (reviewed in [8–10]). Gradients of soluble molecules guide stem cell function regulation within the tissue-specific niche. Reconstitution of the niche signalling environment has until now been tested using microfluidic devices [11] or hydrogel-based 3D structures immobilizing adhesive ligand gradients [12].

Combinatorial and high throughput screening have been used to expose stem cells to arrays of molecule combinations in the search for synergistic effects that could direct cell fate (reviewed in [13]). Authors have mixed together ECM proteins and growth factors and analysed cell phenotype for commitment to certain differentiation paths. One approach was to use functionalized self-assembled monolayers (SAM) to covalently immobilize binary combinations of an adhesive molecule and a growth factor. This method allowed parallel testing of twenty-five environments for control of the fate of neural stem cells [14]. Another approach was to use a multiwell microarray platform that allows 1200 simultaneous experiments on 240 unique signalling environments. Mixtures of ECM proteins were applied using a robotic spotter and mouse embryonic stem cells were cultivated in cocktails of growth factors to identify conditions for generation of cardiac cells. Twenty mixtures of five matrix proteins and twelve cocktails of four growth factors known to modulate cardiac cell differentiation have been thus screened in five replicas [15]. Both approaches were, however, based on previously tested well-defined concentrations of proteins/polymers to obtain combinations thereof. Developmental biology evidence certifies the importance of biomaterials to generate biomolecule gradients in stem-cell driven tissue regeneration [16].

In the field of biomaterials, progress has been made in generating signal gradients to control cell behaviour for tissue regeneration applications (reviewed in [17]). Different gradient polymer surfaces were studied as substrates for cell adhesion, proliferation and gene expression [18]. Biocompatible and biodegradable polysaccharide nanosheets for biomedical application were reported [19]. Levan is a bacterial exopolysaccharide (β2,6-linked fructan) with anti-inflammatory [20], anti-cytotoxic [21] and anti-tumoral [22–24] properties, hence a polymer with potential use in medicine. It has been applied as a thin film by a process called matrix-assisted pulsed laser evaporation (MAPLE) [25]. MAPLE is a soft laser-based technique which is applied to obtain organic nanoscale coatings with specific properties such as adhesion, thickness control and functionality [26–29]. It ensures a great advantage for tissue engineering applications since the method is able to grow very thin nanostructured coatings less than 1 μm thick with improved mechanical properties. This ability allows the avoidance of film cracking or peeling which usually occur when the film is thicker [30] and subsequently make it more difficult to control its dissolution. In the case of polysaccharides films, the adhesion properties are expected to increase because of the high specific surface area of hydrated macromolecules at the interface where they interact and stick to the substrate. We have recently introduced combinatorial-MAPLE (C-MAPLE) as a new method for the fabrication of gradient organic thin films [31] of levan (L) and oxidized levan (OL). When investigated separately, both L and OL MAPLE-deposited thin films showed positive interaction with bone cells that supported cell adhesion and proliferation, critical processes required for tissue regeneration. Moreover, OL thin films generated an increase in cell proliferation as compared to L structures [25]. Following assembly into a compositional gradient, the two polymers generated areas with distinct potential to influence osteoblast cell spreading [31].

Cell response to material cues is mandatory in testing nanostructures' functionality for biomedical applications. For example, in the case of orthopaedic implants, interaction between designed materials and bone cells are first tested *in vitro* [32]. Cell attachment to ECM was shown to control cell cycle [33] with an impact on proliferation kinetics. The sites of interaction between cells and underlying structures are known as focal adhesions, these anchor the cytoskeleton to the ECM. A central role in mediating cell adhesion response to extracellular cues is played by focal adhesion kinase (FAK), which becomes auto-phosphorylated following integrin signalling pathway initiation [34]. Hence, cells sense the environment via integrin receptors that transduce the signals to the cytoskeleton. The adhesion signalling cascade triggers specific gene expression function of substrate physico–chemical features through extracellular signal-regulated kinase (ERK) phosphorylation, a down-stream target of FAK in the mitogen-activated protein kinase (MAPK) pathway [35]. The β1-integrin/FAK/ERK axis was found to be essential for human foetal islet cell differentiation and survival [36]. More precisely, active ERK is targeted at newly forming cell–matrix adhesions [37].

The role of kinases in osteoblast differentiation was recently reviewed [38]. In addition to their role in proliferation and apoptosis, MAPKs were found to be key players in the mechanism of osteoblast differentiation. The mitogen-activated protein kinase family members, ERK, JNK and P38, were shown to contribute to distinct phases of osteogenic differentiation. During *in vitro* osteoblast induction, P38 activation was stimulated from day 9 to day 13 and was associated with initiation of mineral deposition, while activation of JNK was observed later, from day 13 to day 17 and was associated with ECM synthesis and increased calcium deposition by mature osteoblasts. ERK activation was present from day 7 to day 11 and was involved in early commitment to the osteoblast lineage. Blockage of osteogenic differentiation by ERK inhibitors resulted in the adipogenic differentiation of stem cells [39]. ERK was also shown to be essential for human osteoblast growth, integrin expression and function [40, 41]. Moreover, the duration and magnitude of ERK phosphorylation is a determinant factor influencing the early commitment of human bone marrow-derived mesenchymal stem cells to osteogenesis versus adipogenesis [42] or versus chondrogenesis [43].

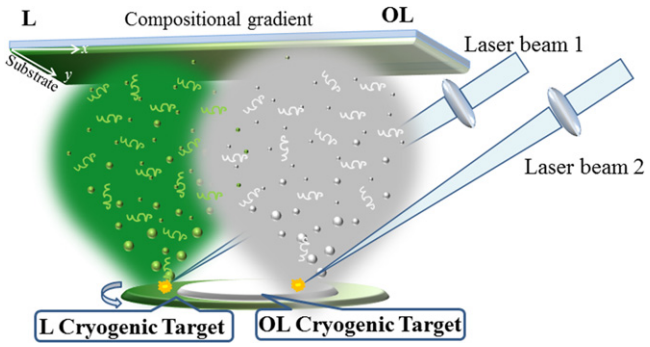

Figure 1. The design of the experimental set-up.

The goal of this study was to evaluate in more detail the response of cells to domains of the combinatorial gradient viewed as distinct signalling entities. We have obtained a continuous reciprocal gradient by combining two biopolymers using C-MAPLE. Interestingly, discrete areas in the gradient surface show different capacities in modulating intracellular signalling events.

2. Materials and methods

2.1. Combinatorial matrix-assisted pulsed-laser evaporation (C-MAPLE)

Fifty milligrams of L and OL were each dissolved in 10 mL of dimethyl sulfoxide (DMSO) to obtain homogeneous solutions. DMSO was selected as the solvent because it does not chemically interact with either L or OL, and absorbs the laser wavelength used for the evaporation of the targets in a frozen state. The solutions were poured into distinct compartments of a ring-like concentric copper holder (see schema in figure 1). This holder has been designed and manufactured to accommodate 5–10 mL of DMSO-based polymer solutions to be used for deposition experiments. Before introduction into the vacuum chamber, the holder containing the solutions was gradually immersed in liquid nitrogen (LN) to obtain two cryogenic targets. These were kept frozen during the deposition process by a cooler, constantly supplied with LN.

In our experiments, a KrF* excimer laser source ($\lambda = 248$ nm, $\tau_{FWHM} = 25$ ns) operating at a repetition rate of 3 Hz was used for target evaporation. The laser beam is divided into two beams by an optical splitter (see figure 1). The distance between the centres of the two laser spots was set at 2 cm. In this configuration, we obtained a 4 cm long polymer co-deposition on glass substrates with the edges containing only L or OL, and continuous gradient areas of L–OL blended composition between [31]. Before deposition, the 17×40 mm^2 glass slides were cleaned in baths of acetone, alcohol and deionized water. Next, they were placed at 4 cm from and parallel to the targets inside a reaction chamber and gently heated at 100 °C. We denote by L the region covered by L only, OL the region covered by OL only, OL–L the intermediary region which we expect to contain more OL than L and L–OL the intermediary region for which we expect more L than OL.

2.2. Morphological investigations using SEM, AFM and fluorescence microscopy

For scanning electron microscopy (SEM) examination, the samples were cut-fragmented after the bottom wafer edge was scratched using a diamond knife. Before SEM, the samples were coated with a very thin layer of gold. The investigations were conducted with a Jeol JSM-5910 LV instrument at 20 kV. An atomic force microscope (AFM; Park systems XE70 SPM controller LSF-100 HS) was used to determine the surface roughness parameters. The probes in noncontact mode were triangular Si_3N_4 cantilevers with integrated tips.

Levan fluorescence was monitored with a Nikon Eclipse E600W epifluorescence microscope with a differential interference contrast (DIC) module and FITC filter. Twin images were captured along the C-MAPLE generated OL–L gradient maintaining the same exposure time for detection of fluorescence emission between specimens.

2.3. Contact angle measurements

Contact angle (CA) measurements were carried out using a Krüss DSA-100 model CA meter equipped with a single direct dosing system consisting of a High Performance Frame Grabber Camera T1C (25 frames per second) and controlled by DS3210 software (providing the static and dynamic operation modes). The CA values were determined using the sessile drop technique. Two 1 μL drops of distilled water were dropped onto the surface using the autodosing system. Static CA measurements were performed immediately after the formation of sessile drops of liquid on the surface.

2.4. Osteoblast attachment assay

Human osteoblast-like SaOs2 cells (a kind gift from Dr Karine Anselme) were cultured in DMEM supplemented with 10% FCS (Biochrom AG), 1% Glutamax, 50 U mL^{-1} penicillin and 50 mg mL^{-1} streptomycin (Gibco). Cells were split every 3–4 days (1:3) and cultured in a 5% CO_2 humid atmosphere at 37 °C.

C-MAPLE polymer gradients were obtained on glass collectors that were cut into four equal regions denoted as OL, OL–L, L–OL, and L. Before cell culture, samples were placed in 6-well plates and sterilized by incubation in 1% penicillin–streptomycin solution for 2 h, followed by two washes in PBS.

Cells at approximately 70% confluence were washed twice with PBS and starved for 16 h in a serum-free medium before the experiment. SaOs2 cells were detached using 0.2% EDTA in PBS, centrifuged and resuspended in a serum-free medium for counting (lack of serum assures no interference by adhesion protein adsorption in cell attachment). Fifty thousand cells were seeded per sample in duplicates and incubated at 37 °C for 40 min. For western blotting, osteoblasts were scraped in cold PBS and lysed in 25 μL RIPA buffer containing 1% NP-40, and supplemented with

Complete protease (Roche) and phosphatase inhibitors. For immunofluorescence (IF), non-adhered cells were removed by PBS washes; samples were fixed in 4% p-formaldehyde and kept in PBS at 4 °C before labelling. Fixed cells were permeabilized by 0.3% Triton-X-100 treatment. Actin filaments were labelled with Alexa Fluor 488-conjugated Phalloidin (Invitrogen) in 1% BSA–0.3% Triton X-100. The samples were washed three times with PBS and mounted using Prolong antifade with DAPI (Invitrogen). For attachment efficiency determinations, cells were analysed using a Zeiss upright Axio Imager microscope with an ApoTome slider module. Attached cells were counted in five different fields and image analysis was performed using Image J. Data are presented as means ± s.e.m.

2.5. Immunoblotting

Cell lysates obtained 40 min after attachment were clarified by centrifugation and denatured by boiling for 5 min at 95 °C in a loading buffer with DTT. Samples were run in an 8% SDS-PAGE gel and transferred onto Immobilon-FL PVDF membranes (Millipore). After blocking for 1 h in 2% ECL Advanced (GE Healthcare) in 0.1% TBS-T, an overnight incubation at 4 °C with rabbit anti-pERK antibodies (cell signaling) in 5% BSA (Santa Cruz) was performed. The next day, the membrane was thoroughly washed and probed with Cy5-conjugated anti-rabbit antibodies at 1:2500 dilution in ECL Advanced. The membrane was finally washed and scanned using Typhoon FLA9500 (GE Healthcare) and appropriate filters at a resolution of 100 μm. For total protein normalization, the membrane was reprobed with mouse anti-actin antibodies (abcam) following a classical protocol and ECL Femto detection (Thermo Pierce). Specific pERK1/2 and β-actin bands were quantified by densitometry using Image Quant TL (GE Healthcare) and Quantity One (Bio-Rad) softwares, respectively. One representative experiment is presented of the three performed.

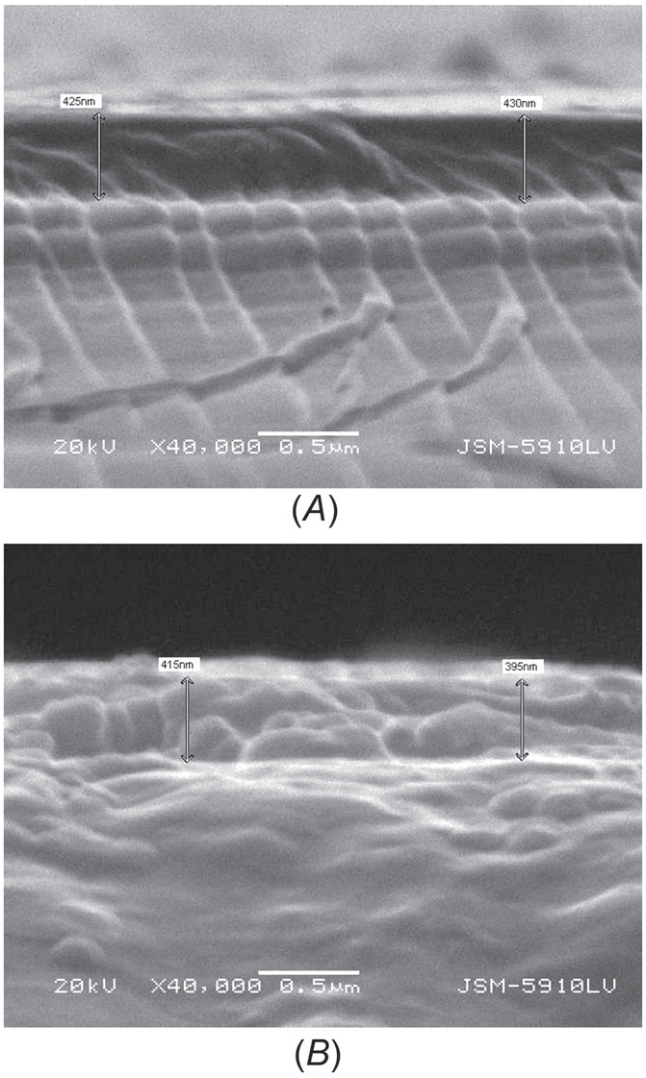

Figure 2. Typical XSEM images of different combinatorial thin film regions: (*A*) cross view (zone OL) and (*B*) tilted view (zone OL–L).

3. Results and discussion

3.1. Morphological characteristics

We present in figures 2(*A*) and (*B*) typical XSEM images from which we were able to estimate the film uniformity and thickness as well as validate the adhesion of C-MAPLE polymer composite coatings. We grew homogenous films along the glass slide from the L to OL regions, with a constant average thickness of approximately 400 ± 50 nm. The obtained composite structure is composed of spherical polymer globules, as are visible in figure 2(*B*). Next, we made use of levan autofluorescence (figure 3(*A*), 40 × levan/glass images) to qualitatively assess the existence of a compositional gradient along the obtained thin film as already observed by Fourier transform infrared microspectroscopy in our previous study [31]. Figure 3 provides evidence that a gradual increase in autofluorescence consistent with a gradual increase in L concentration is indeed observed along the glass slide collector. As is known [44], L contains fructose and is highly fluorescent under excitation at 488 nm while OL loses the fluorescence by fructose oxidation to aldehyde groups. Images taken under an epifluorescence microscope swapping between DICs (figure 3(*A*) top row) and green fluorescence modes (figure 3(*A*) bottom row) confirm the expected compositional gradient (figure 3(*B*)). An empty glass negative control showed no autofluorescence on the green fluorescence channel at the exposure time used (figure 3(*A*) left). The images were analysed and a graph of fluorescence intensity was drawn which supports the progressive increase in fluorescence with an increase in levan concentration (figure 3(*C*)).

3.2. C-MAPLE films' surface features

The CA of a sessile drop varies not only with physical texture or roughness, but also with chemical texture determined by the composition of the solid surface [45]. We hypothesize that by the modification of the chemical composition from L to

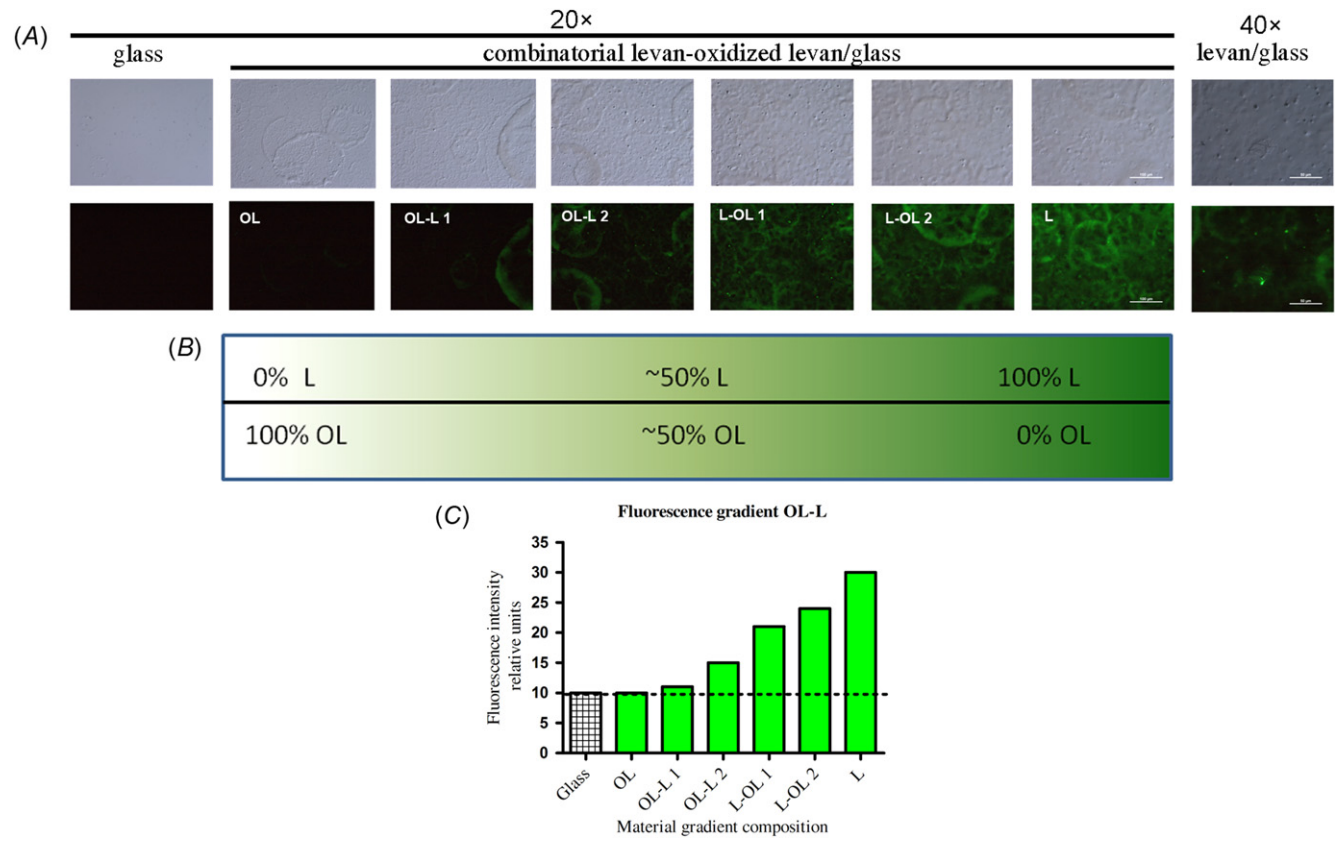

Figure 3. (*A*) Differential interference contrast images and fluorescence microscopy evaluation of OL–L (left and right respectively) gradient film obtained by C-MAPLE along the glass slide. Positive (levan/glass) and negative (glass) controls are presented. Bar = 100 μm (20×) and 50 μm (40×). (*B*) Diagram of expected composition gradient obtained by C-MAPLE from OL and L targets. (*C*) Quantification of gradient regions' fluorescence emission intensity using the ImageJ histogram function. The glass background is set as the threshold and depicted as a dotted line.

OL, the physical and chemical parameters generate the CA non-linear variation.

To discriminate between the actions of the two factors, we recorded the roughness parameters along the sample using AFM. It was observed that the obtained coatings are quite smooth with similar rms and Ra values below 2 nm. The roughness parameters present quite comparable values with a noticeable decrease in the OL–L region (figure 4(*A*)). It is known that a water droplet can assemble on a surface in two different configurations: (i) the Wenzel state, which is conformal with the topography and (ii) the Fakir (also known as the Cassie–Baxter) state, which is not conformal with the topography and only touches the peaks of the protrusions on the surface [46]. It follows that the Wenzel state actually describes our gradient structure since the less hydrophilic surface exhibits a small roughness. As a matter of fact, the CA reaches its maximum (~80 degrees) in the zone OL–L (figure 4(*B*)), where the roughness was the smallest (figure 4(*A*)), which is characteristic for hydrophobic surfaces. The rougher the surface the smaller the CA, as the droplet either pursues the topography or it penetrates inside the texture [47].

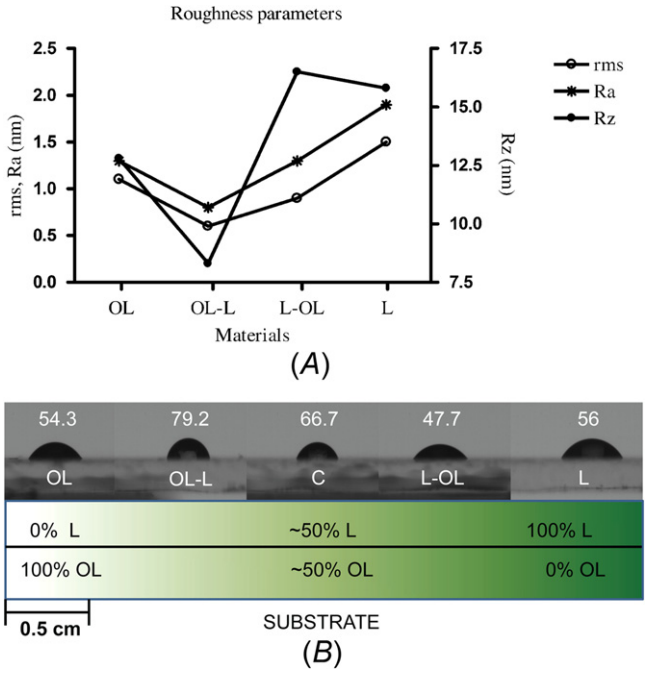

Figure 4. (*A*) Roughness evaluation along the length of the combinatorial L–OL sample by AFM. (*B*) CA values for the representative regions along the length of the combinatorial L–OL sample.

3.3. Efficiency of bone cell attachment along C-MAPLE levan gradient films

There is increased interest in obtaining cell instructive materials that could control and regulate cell fate for biomedical and research applications [48]. Coating surfaces with gradient thin films of biomolecules allows the construction of an array of different chemical and physical features. Cells can be exposed to combinatorial nanostructures to screen for specific conditions in order to direct their fate towards specific phenotypes.

The primary steps in the cell–substrate interaction of anchorage-dependent cells are represented by cell attachment, followed by adhesion and proliferation. Investigation of early cell attachment efficiency and morphology is, therefore, indicative of material biocompatibility. At this stage, cells are developing microvilli, which are cytoplasmic structures that make contact with the surface by means of physico–chemical bonds, such as ionic and van der Waals forces. Next, during adhesion, complex interaction between cell-produced ECM (consisting of ligands such as collagen and fibronectin (FN)), plasma membrane embedded proteins (integrin receptors) and cytoskeleton (actin filaments) dictates cell fate [49]. As a consequence of integrin-mediated cell adhesion to ECM, intracellular signalling pathways are activated. These trigger specific gene expressions which control cell morphology, proliferation and finally differentiation. During this stage, cell spreading occurs which leads to an increase in contact area [50].

We have previously reported productive interactions of osteoblasts with MAPLE films obtained from L and OL [25] as well as with C-MAPLE films synthesized from the two organic macromolecules [31] which favoured cell adhesion and proliferation. These studies revealed that cells prefer to proliferate on OL rather than L layers whether deposited singly or in compositional gradients. Surprisingly, a significant accumulation of cells onto L–OL regions was observed after three days of osteoblast culture [31] which could be related to increased surface wettability. Another explanation could be associated with the presence of the appropriate amount of OL within L coatings which in turn means that the degree of oxidation plays an essential role in the bioactivity of the structures obtained. The combined effects of hydrophilicity, chemical composition (OL presence) and roughness parameters can account for the improved bone cell proliferation on the L–OL and OL zones. It is very important to note that cell proliferation on OL-based materials was superior to standard glass cover slips.

To elucidate how compositional variance affects the initial cell–biomaterial interactions, we investigated the effect of the OL–L gradient on early cell attachment. Samples were cut into four equal regions (OL, OL–L, L–OL and L respectively) to test differences in cell attachment along the combinatorial gradient. Forty minutes after seeding the pre-starved SaOs2 cells in the serum-free conditions, the fluorescence microscopy results showed a direct relationship between OL proportion and number of attached cells (figures 5(*A*) and (*B*)). Peripheral lamaellipodia and transversal actin stress fibres, comparable to cells cultured on FN (data not shown), are visible in the case of cells attached to OL (figure 5(*A*)). Cell spreading decreases with a decrease in OL fraction as previously observed during a longer 72 h adhesion experiment [31]. This could be linked to the extreme values of wettability (CA = 79.2 for OL–L and CA = 47.7 for L–OL as opposed to CA = 54.3 for OL, see figure 3(*A*)), as it is already accepted that moderate hydrophylicity/

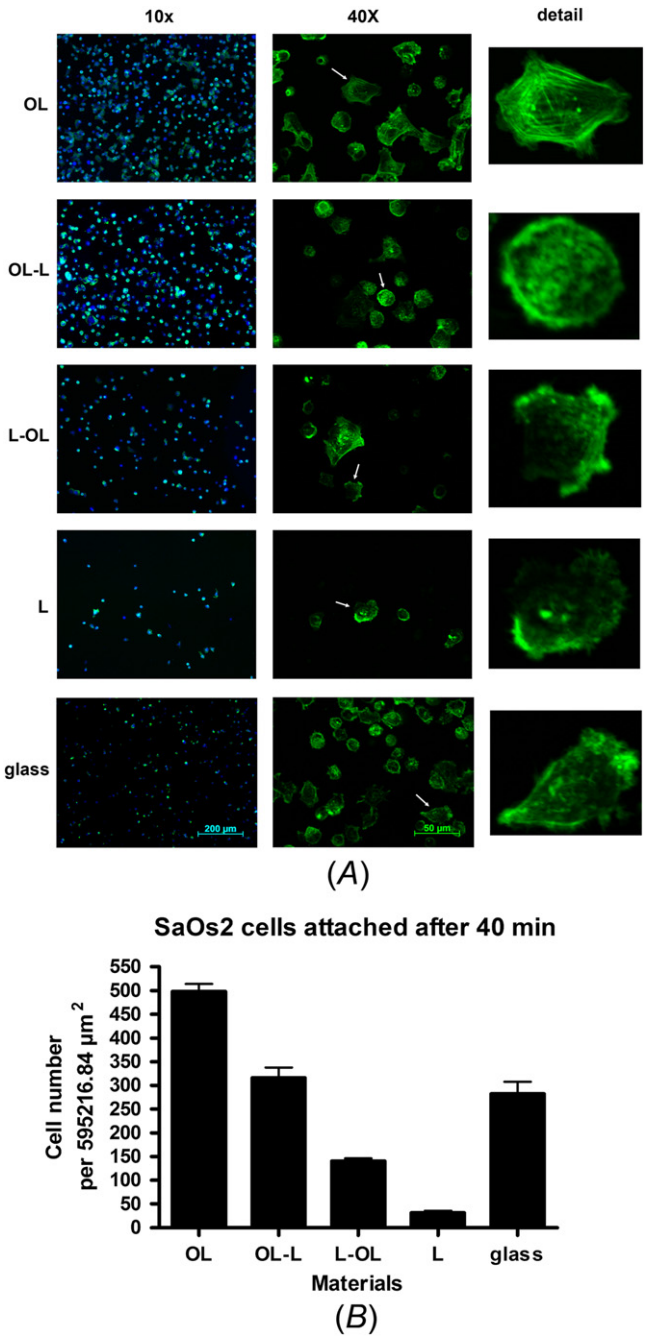

Figure 5. (*A*) Fluorescence microscopy of SaOs2 cells 40 min post-attachment on combinatorial and control materials. Different magnifications of cells labelled with Alexa Fluor 488-conjugated phalloidin (actin, green) and DAPI (nuclei, blue) are shown together with morphological details of cells marked by white arrows. (*B*) Quantification of the cell number of five 10× fields using the ImageJ nuclei counting function. Mean ± s.e.m. is depicted on the graph.

hydrophobicity favours cell-substrate interaction [51]. Studies performed on self-assembled monolayers with well-defined chemistry and a wide range of wettability values have shown that wettability is the primary determinant of cell adhesion, but this process is also affected by the surface functional group, surface density and cell type [52]. More recent research concluded that cell adhesion is determined by the synergy of the roughness degree and surface chemistry, which determines the wettability [53]. Filopodia were the preponderant structures developing at the plasma membrane on the OL–L, L–OL and L regions. Moderate cell attachment was found on glass (figure 5(*B*)).

3.4. C-MAPLE L gradient films signalling to human osteoblasts

Adhesion complexes are signalling hubs [54] that integrate signals from the microenvironment and translocate them into the cells to modulate gene expression and consequently cell function. During early attachment, FAK was found to strengthen cell adhesion via integrin receptor activation. This function is later associated with vinculin recruitment to focal adhesions [55]. It is widely acknowledged that integrin-mediated cell adhesion, in the absence of soluble factors, can directly lead to the activation of the MAPK cascade [56], downstream of FAK phosphorylation [57, 58].

Next, we used bone cells as live sensors of the molecular environment and quantified ERK1/2 activation following cell attachment by immunoblotting of cell lysates in parallel with the fluorescence microscopy experiment. This complementary assay showed an enhanced phosphorylation of ERK1/2 during early attachment of starved SaOs2 cells on OL–L and L–OL materials as compared to OL or L alone and the control bare glass surface (figures 6(*A*) and (*B*)). We advance the hypothesis that ERK1/2 activation compensates for a decreased attachment rate (figures 6(*A*) and (*B*)) of these combinatorial zones, which results in similar material surface coverage long-term [25].

As known, L manifests its immunostimulating effect via pattern recognition by Toll-like receptor 4 (TLR4) [59], which has also been found to be expressed by SaOs2 osteoblasts [60]. Apart from being activated by integrin stimulation, ERK1/2 is sensitive to TLR4-mediated signalling [61, 62]. Hence, an integrated response to both L chemistry and surface cues as sensed by cell receptors (TLR4 and integrins, respectively) could result in different levels of ERK1/2 phosphorylation in SaOs2 cells attached to C-MAPLE L/OL films.

It has already been proven that nanotopographical cues modulate ERK signalling of skeletal stem cells [63] with potential implications for osteogenesis [41]. The ERK-dependent expression of osteogenic transcription factor Runx2 was described in bone marrow mesenchymal stem cells under continuous mechanical strain leading to cell differentiation [64].

A recent study has succeeded for the first time in reprogramming cells using cocktails of seven small molecules selected from a 10 000 compound library [65]. This is an alternative to the genetic manipulation or nuclear transfer

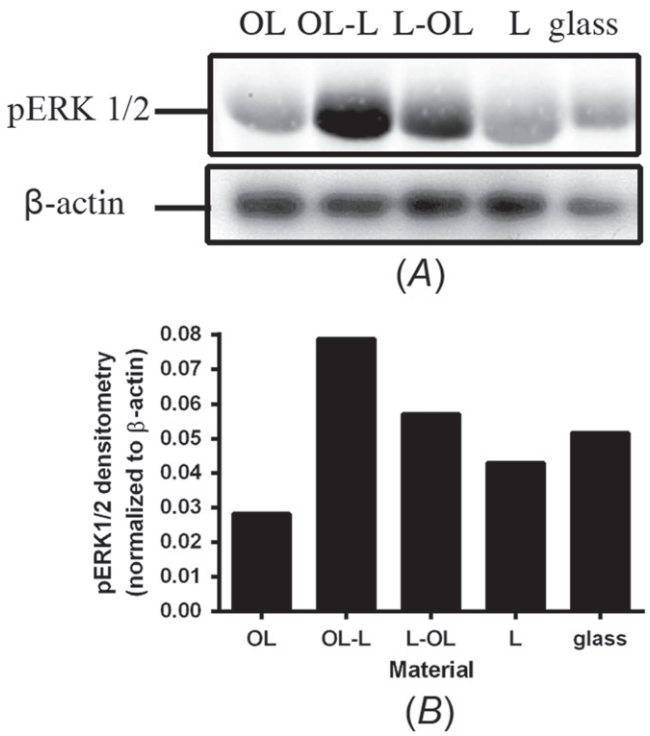

Figure 6. (*A*) Immunoblotting analysis of pERK1/2 expression. Anti-*β*-actin antibodies were used for normalization to total loaded protein. (*B*) Densitometry results of pERK 1/2 normalized to *β*-actin expression by Image Quant TL and Quantity One gel analysis, respectively.

used up to now to generate induced pluripotent stem cells. Epigenetic control of cell fate using specific combinations of molecules is an attractive strategy for future clinical applications. From this perspective our proposed C-MAPLE generated combinatorial gradient has, in our opinion, remarkable potential in the screening of new bioactive interfaces for tissue regeneration.

4. Conclusions

We found that the modification of chemical composition in the L–OL binary system and surface physical texture stayed at the origin of CA variance. A biological effect was evidenced consisting in improved accumulation of cells on film regions (different from the two ends), as compared with all other film areas, which in turn is most probably connected to surface wettability and an appropriate degree of polymer oxidation.

The cell signalling response to the surface composition gradient and roughness has shown that combinations of OL and L (OL–L and L–OL) increase ERK activation as compared to OL or L alone. The analyses revealed a structure–function relationship and beneficial design guidelines. This basically refers to the existence of an optimum mixture between the OL and L constituents, and more or less hydrophilic areas. Once identified, the optimum region could be recognized by rapid fluorescence microscopy scanning. The generation of smart, discrete materials with desired

properties such as the rate of coating dissolution is a prospective, challenging task.

In conclusion, we have shown here that by combining two biopolymers with different oxidation states a compositional gradient can be obtained with micro-areas that modulate the ERK signalling of osteoblasts. This method can be further developed for the screening of specific dosages of combined signalling molecule mixtures that could guide cell fate towards the phenotypes required for tissue regeneration.

Acknowledgements

This work was supported by the bilateral contracts 112M330 and 597/2013 between Turkey and Romania. CR, FS, NS and INM acknowledge the support of UEFISCDI under the contract TE 82/2011. FS and LES acknowledge financial support from the European Social Fund POSDRU 2007-2013 through the contract POSDRU/89/1.5/S/60746.

References

[1] Hench L L and Polak J M 2002 Third-generation biomedical materials *Science* **295** 1014–7
[2] Holzapfel B M *et al* 2013 How smart do biomaterials need to be? A translational science and clinical point of view *Adv. Drug. Deliv. Rev.* **65** 581–603
[3] Stevens M M and George J H 2005 Exploring and engineering the cell surface interface *Science* **310** 1135–8
[4] Szpalski C, Wetterau M, Barr J and Warren S M 2012 Bone tissue engineering: current strategies and techniques: I. scaffolds *Tissue Eng. Part B Rev.* **18** 246–57
[5] Hwang N S, Varghese S and Elisseeff J 2008 Controlled differentiation of stem cells *Adv. Drug. Deliv. Rev.* **60** 199–214
[6] Fu R H *et al* 2011 Differentiation of stem cells: strategies for modifying surface biomaterials *Cell Transplant* **20** 37–47
[7] Martino S, D'Angelo F, Armentano I, Kenny J M and Orlacchio A 2012 Stem cell-biomaterial interactions for regenerative medicine *Biotechnol. Adv.* **30** 338–51
[8] Pennesi G, Scaglione S, Giannoni P and Quarto R 2011 Regulatory influence of scaffolds on cell behavior: how cells decode biomaterials *Curr. Pharm. Biotechnol.* **12** 151–9
[9] Lutolf M P and Hubbell J A 2005 Synthetic biomaterials as instructive extracellular microenvironments for morphogenesis in tissue engineering *Nat. Biotechnol.* **23** 47–55
[10] Lutolf M P and Blau H M 2009 Artificial stem cell niches *Adv. Mater* **21** 3255–68
[11] Chung B G *et al* 2005 Human neural stem cell growth and differentiation in a gradient-generating microfluidic device *Lab Chip* **5** 401–6
[12] Burdick J A, Khademhosseini A and Langer R 2004 Fabrication of gradient hydrogels using a microfluidics/photopolymerization process *Langmuir* **20** 5153–6
[13] Fisher O Z, Khademhosseini A, Langer R and Peppas N A 2010 Bioinspired materials for controlling stem cell fate *Acc. Chem. Res.* **43** 419–28
[14] Nakajima M *et al* 2007 Combinatorial protein display for the cell-based screening of biomaterials that direct neural stem cell differentiation *Biomaterials* **28** 1048–60
[15] Flaim C J, Teng D, Chien S and Bhatia S N 2008 Combinatorial signaling microenvironments for studying stem cell fate *Stem Cells Dev.* **17** 29–39
[16] Lutolf M P, Gilbert P M and Blau H M 2009 Designing materials to direct stem-cell fate *Nature* **462** 433–41
[17] Wu J, Mao Z, Tan H, Han L, Ren T and Gao C 2012 Gradient biomaterials and their influences on cell migration *Interface Focus* **2** 337–55
[18] Kim M, Khang G and Lee H 2008 Gradient polymer surfaces for biomedical applications *Prog. Polym. Sci.* **33** 138–64
[19] Fujie T, Matsutani N, Kinoshita M, Okamura Y, Saito A and Takeoka S 2009 Adhesive, flexible, and robust polysaccharide nanosheets integrated for tissue-defect repair *Advanced Functional Materials* **19** 2560–8
[20] Kim K H, Chung C B, Kim Y H, Kim K S, Han C S and Kim C H 2005 Cosmeceutical properties of levan produced by Zymomonas mobilis *J. Cosmet. Sci.* **56** 395–406
[21] Poli A *et al* 2009 High level synthesis of levan by a novel halomonas species growing on defined media *Carbohydrate Polymers* **78** 651–7
[22] Yoo S H, Yoon E J, Cha J and Lee H G 2004 Antitumor activity of levan polysaccharides from selected microorganisms *Int. J. Biol. Macromol.* **34** 37–41
[23] Calazans G M T, Lima R C, de Franca F P and Lopes C E 2000 Molecular weight and antitumour activity of zymomonas mobilis levans *Int. J. Biol. Macromol.* **27** 245–7
[24] Leibovici J and Stark Y 1984 Direct antitumor effect of the polysaccharide levan in mice: effects of drug concentration and time and temperature of incubation *J. Natl. Cancer. Inst.* **72** 1417–20
[25] Sima F *et al* 2011 Levan nanostructured thin films by MAPLE assembling *Biomacromolecules* **12** 2251–6
[26] Chrisey D B *et al* 2003 Laser deposition of polymer and biomaterial films *Chem. Rev.* **103** 553–76
[27] Guo Y *et al* 2012 Ultrastable nanostructured polymer glasses *Nat. Mater.* **11** 337–43
[28] Mihaiescu D E *et al* 2013 Functionalized magnetite silica thin films fabricated by MAPLE with antibiofilm properties *Biofabrication* **5** 015007
[29] Dinca V *et al* 2013 MAPLE-based method to obtain biodegradable hybrid polymeric thin films with embedded antitumoral agents *Biomed. Microdevices* **16** 11–21
[30] Kim S S and Hyun J C 2001 Drying of coated film *Handbook of Solvents* ed G Wypych (Norwich, NY: William Andrew) p 410
[31] Sima F *et al* 2012 Combinatorial matrix-assited pulsed laser evaporation: single-step synthesis of biopolymer compositional gradient thin film assemblies *Appl. Phys. Lett.* **101** 233705–9
[32] Anselme K 2000 Osteoblast adhesion on biomaterials *Biomaterials* **21** 667–81
[33] Bao W, Thullberg M, Zhang H, Onischenko A and Stromblad S 2002 Cell attachment to the extracellular matrix induces proteasomal degradation of p21(CIP1) via Cdc42/Rac1 signaling *Mol. Cell. Biol.* **22** 4587–97
[34] Parsons J T, Martin K H, Slack J K, Taylor J M and Weed S A 2000 Focal adhesion kinase: a regulator of focal adhesion dynamics and cell movement *Oncogene* **19** 5606–13
[35] Owen G R, Meredith D O, ap Gwynn I and Richards R G 2005 Focal adhesion quantification—a new assay of material biocompatibility? Review *Eur. Cells Mater.* **9** 85–96
[36] Saleem S, Li J, Yee S P, Fellows G F, Goodyer C G and Wang R 2009 Beta1 integrin/FAK/ERK signalling pathway is essential for human fetal islet cell differentiation and survival *J. Pathol.* **219** 182–92
[37] Fincham V J, James M, Frame M C and Winder S J 2000 Active ERK/MAP kinase is targeted to newly forming cell-matrix adhesions by integrin engagement and v-Src *EMBO J.* **19** 2911–23

[38] Matsuguchi T 2012 Roles of kinases in osteoblast function *Advances in Protein Kinases* ed G Da Silva Xavier (Rijeka: InTech)
[39] Jaiswal R K, Jaiswal N, Bruder S P, Mbalaviele G, Marshak D and Pittenger M F 2000 Adult human mesenchymal stem cell differentiation to the osteogenic or adipogenic lineage is regulated by mitogen-activated protein kinase *J. Biol. Chem.* **275** 9645–52
[40] Lai C F *et al* 2001 ERK is essential for growth, differentiation, integrin expression, and cell function in human osteoblastic cells *J. Biol. Chem.* **276** 14443–50
[41] Ge C, Xiao G, Jiang D and Franceschi R T 2007 Critical role of the extracellular signal-regulated kinase-MAPK pathway in osteoblast differentiation and skeletal development *J. Cell Biol.* **176** 709–18
[42] Jung H S, Kim Y H and Lee J W 2011 Duration and magnitude of extracellular signal-regulated protein kinase phosphorylation determine adipogenesis or osteogenesis in human bone marrow-derived stem cells *Yonsei Med. J.* **52** 165–72
[43] Pelaez D, Arita N and Cheung H S 2012 Extracellular signal-regulated kinase (ERK) dictates osteogenic and/or chondrogenic lineage commitment of mesenchymal stem cells under dynamic compression *Biochem. Biophys. Res. Commun.* **417** 1286–91
[44] Gordon E M, Gallop M A and Patel D V 1996 Strategy and tactics in combinatorial organic synthesis. Applications to drug discovery *Acc. Chem. Res.* **29** 144–54
[45] Zhang J and Han Y 2008 A topography/chemical composition gradient polystyrene surface: toward the investigation of the relationship between surface wettability and surface structure and chemical composition *Langmuir* **24** 796–801
[46] Shastry A, Case M J and Bohringer K F 2005 Engineering surface roughness to manipulate droplets in microfluidic systems *2005 MEMS, 18th IEEE Conf. Publ.* pp 694–7
[47] Bico J, Thiele U and Quéré D 2002 Wetting of textured surfaces *Colloids Surf.* A **206** 41–6
[48] Ventre M, Causa F and Netti P A 2012 Determinants of cell-material crosstalk at the interface: towards engineering of cell instructive materials *J R Soc Interface* **9** 2017–32
[49] Brunton V G, MacPherson I R and Frame M C 2004 Cell adhesion receptors, tyrosine kinases and actin modulators: a complex three-way circuitry *Biochim. Biophys. Acta* **1692** 121–44
[50] Zinger O *et al* 2004 Time-dependent morphology and adhesion of osteoblastic cells on titanium model surfaces featuring scale-resolved topography *Biomaterials* **25** 2695–711
[51] Bacakova L, Filova E, Rypacek F, Svorcik V and Stary V 2004 Cell adhesion on artificial materials for tissue engineering *Physiol. Res.* **53** S35–45
[52] Arima Y and Iwata H 2007 Effect of wettability and surface functional groups on protein adsorption and cell adhesion using well-defined mixed self-assembled monolayers *Biomaterials* **28** 3074–82
[53] Ranella A, Barberoglou M, Bakogianni S, Fotakis C and Stratakis E 2010 Tuning cell adhesion by controlling the roughness and wettability of 3D micro/nano silicon structures *Acta Biomater.* **6** 2711–20
[54] Byron A 2011 Analyzing the anatomy of integrin adhesions *Sci. Signal.* **4** jc3
[55] Michael K E, Dumbauld D W, Burns K L, Hanks S K and Garcia A J 2009 Focal adhesion kinase modulates cell adhesion strengthening via integrin activation *Mol. Biol. Cell* **20** 2508–19
[56] Aplin A E, Howe A, Alahari S K and Juliano R L 1998 Signal transduction and signal modulation by cell adhesion receptors: the role of integrins, cadherins, immunoglobulin-cell adhesion molecules, and selectins *Pharmacol. Rev.* **50** 197–263
[57] Mitra S K, Hanson D A and Schlaepfer D D 2005 Focal adhesion kinase: in command and control of cell motility *Nat. Rev. Mol. Cell Biol.* **6** 56–68
[58] Yee K L, Weaver V M and Hammer D A 2008 Integrin-mediated signalling through the MAP-kinase pathway *IET Syst. Biol.* **2** 8–15
[59] Xu Q, Yajima T, Li W, Saito K, Ohshima Y and Yoshikai Y 2006 Levan (beta-2, 6-fructan), a major fraction of fermented soybean mucilage, displays immunostimulating properties via Toll-like receptor 4 signalling: induction of interleukin-12 production and suppression of T-helper type 2 response and immunoglobulin E production *Clin. Exp. Allergy* **36** 94–101
[60] Asai Y, Hirokawa Y, Niwa K and Ogawa T 2003 Osteoclast differentiation by human osteoblastic cell line SaOS-2 primed with bacterial lipid A *FEMS Immunol. Med. Microbiol.* **38** 71–9
[61] Fan H, Peck O M, Tempel G E, Halushka P V and Cook J A 2004 Toll-like receptor 4 coupled GI protein signaling pathways regulate extracellular signal-regulated kinase phosphorylation and AP-1 activation independent of NFkappaB activation *Shock* **22** 57–62
[62] Kawai T and Akira S 2010 The role of pattern-recognition receptors in innate immunity: update on Toll-like receptors *Nat. Immunol.* **11** 373–84
[63] Biggs M J, Richards R G, Gadegaard N, Wilkinson C D, Oreffo R O and Dalby M J 2009 The use of nanoscale topography to modulate the dynamics of adhesion formation in primary osteoblasts and ERK/MAPK signalling in STRO-1+ enriched skeletal stem cells *Biomaterials* **30** 5094–103
[64] Zhang P, Wu Y, Jiang Z, Jiang L and Fang B 2012 Osteogenic response of mesenchymal stem cells to continuous mechanical strain is dependent on ERK1/2-Runx2 signaling *Int. J. Mol. Med.* **29** 1083–9
[65] Hou P *et al* 2013 Pluripotent stem cells induced from mouse somatic cells by small-molecule compounds *Science* **341** 651–4